Title:

Jagged1 is a Notch-independent mechanotransducer in endothelial cells

Authors:

Freddy Suarez Rodriguez[1,2,3], Noora Virtanen[1,2,3], Elmeri Kiviluoto[1,2,3], Rob C. H. Driessen[4,5], Feihu Zhao[6], Carlijn V. C. Bouten[4,5], Oscar M. J. A. Stassen[1,4], Cecilia M. Sahlgren[1,2,3,4,5]

Affiliations:

[1]Faculty of Science and Engineering, Cell Biology, Åbo Akademi University; Turku, Finland.

[2]Turku Bioscience, Åbo Akademi University and University of Turku; Turku, Finland.

[3]InFLAMES Research Flagship Center, Åbo Akademi University and University of Turku; Turku, Finland.

[4]Department of Biomedical Engineering, Eindhoven University of Technology; Eindhoven, the Netherlands.

[5]Institute for Complex Molecular Systems (ICMS), Eindhoven University of Technology; Eindhoven, the Netherlands.

[6]Department of Biomedical Engineering, Zienkiewicz Institute for Modelling, Data & AI, Faculty of Science and Engineering, Swansea University; Swansea, United Kingdom.

*Corresponding author. Email: cecilia.sahlgren@abo.fi.

Abstract:

Fluid shear stress (FSS) from the blood flow is a crucial regulator of vascular physiology and is associated with major cardiovascular pathologies. Endothelial cells are the primary mechanotransducers of FSS. Here, we show that Jagged1, a canonical ligand of the Notch pathway, modulates biomechanical signaling in endothelial cells in response to FSS. We found that changes in FSS magnitude alter the expression and localization of Jagged1 independently of its effect on Notch expression or activation. Deletion of Jagged1 decreases FSS-induced VEGFR2 and ERK activity in vitro and causes attenuated kinase activity and cardiac defects in zebrafish embryos without significant changes in canonical Notch activity. We show that direct physical stimulation of Jagged1 induces mechanosignaling through the VEGFR2 pathway, independently of Notch signaling but mediated by Jagged1-induced Src activation. Our findings suggest a novel non-canonical role for Jagged1 as a mechanotransducer in endothelial cells with implications for cardiovascular morphogenesis and disease.

One Sentence Summary:

Jag1 activates endothelial mechanosignaling through Src.

Main Text:

INTRODUCTION

Mechanical forces generated by blood flow direct cardiovascular morphogenesis, homeostasis, and disease progression (1, 2). Endothelial cells lining the lumen of cardiovascular tissues are exposed to fluid shear stress (FSS), which is an essential signal for vasculogenesis, angiogenesis, arterial specification, vessel maturation, and barrier function (1, 3, 4). FSS is also a well-known predictor of atherosclerotic plaque formation, with zones of lower magnitude of FSS and higher oscillatory shear index (OSI) being atheroprone, and those with laminar-like (low OSI) and higher magnitudes of FSS considered atheroprotective (1, 4, 5). Physiological FSS varies in different vessels, typically ranging from magnitudes as low as 0.4 Pa to as high as 7 Pa (1, 6, 7). Endothelial cells express mechanosensors such as the primary cilium, the glycocalyx, Piezo ion channels, the VEGFR2 - VE-cadherin - PECAM junctional mechanosensory complex, and PlexinD1, which activate downstream signaling regulating endothelial cell responses to FSS (8–10).

The Notch signaling pathway is a crucial regulator of cardiovascular development and homeostasis (11–13). Notch plays an important role in angiogenesis, arterial specification, endothelial barrier function, cardiac morphogenesis, and arterial remodeling (12, 14–18). In canonical Notch signaling, Notch ligands on the membrane of signal-sending cells bind and activate Notch receptors on signal-receiving cells. The activated receptor is then cleaved, and its intracellular domain is translocated to the nucleus, where it promotes the transcription of Notch target genes (19). Notch activity is sensitive to mechanical signals both directly and indirectly, and the regulation of Notch signaling is essential for the cellular response to hemodynamic stress (11, 20–22). Laminar-like and high magnitude (~2 Pa) FSS has been shown to induce Notch1 activation (23, 24), while high OSI of high (1.5 Pa) and low (0.4 Pa) magnitude has been found to stimulate Notch3 and Notch4, respectively (25, 26).

FSS induces Notch1 activity in arteries, which promotes vascular barrier integrity (16) and serves an atheroprotective role in regions exposed to high laminar blood flow (~2 Pa) (24). In contrast to Notch1, recent data suggest that the Notch ligand Jagged1 (Jag1) is enriched in pro-atherogenic zones, of FSS with low magnitude (~0.4 Pa) and high OSI (26, 27), and promotes atherosclerosis (26). Here, we investigated the flow-responsive nature of Jag1. We show that magnitude-specific changes in FSS tune Jag1 expression and localization and identify a non-canonical role of Jag1 in regulating the activity of FSS-responsive kinases.

RESULTS

Shear stress induces polarization and magnitude-dependent Jag1 expression

To elucidate the influence of FSS on Jag1, we exposed endothelial cells to different magnitudes of FSS using parallel plate microfluidic chips. FSS induced distinct relocalization of Jag1 into subcellular vesicles and a polarized distribution in the flow direction in endothelial cells exposed to 1.4 Pa for 24 hours in both human aortic endothelial cells (HAECs) and human umbilical vein endothelial cells (HUVEC) (Fig. 1A, and fig. S1). A similar polarization has previously been observed for Notch1, at a higher magnitude of 2.6 Pa (24).

Since Notch has been shown to respond to low OSI (laminar-like) FSS ranging from 0.3 Pa to over 2 Pa (16, 23, 24), we next tested the influence of various FSS levels,

ranging from 0 to 2 Pa at low OSI, on Jag1 expression. To this end, we used an orbital shaker to complement the microfluidic chips and obtain sufficient material for further protein analysis. We utilized computational fluidic dynamics to characterize FSS magnitude and OSI in a 6-well cell culture plate (Fig. 1B) to be able to isolate cells exposed to laminar-like flow with low OSI (Fig. 1C) and specific magnitude of FSS (Fig. 1D) as previously described (28). FSS induced an increase in Jag1 protein (Fig. 1E) and mRNA (Fig. 1F) expression, and the levels peaked around 0.8-1 Pa. The Jag1 expression pattern did not match the expression pattern of Notch receptors and Notch ligand Dll4 (fig. S2), and did not correlate with Notch activation by FSS, which has been reported to increase up to 2 Pa (23) and beyond (24). Jag1 expression increased the first six hours under ~0.8 Pa laminar-like FSS and the expression was then maintained for the duration of the experiment (24hrs) (fig. S3). In contrast, Notch1 expression has been reported to peak at 12 hours after onset of flow and then decrease (24). To evaluate the impact of FSS pattern on Jag1 expression, we examined the expression of Jag1 and other Notch signaling genes across a transition from continuous to pulsatile flow. This shift in FSS pattern resulted in increased Notch1 expression and alterations in its downstream targets, HES1 and HEY1, while no changes were observed in Jag1 expression (fig. S4).

Endothelial Jag1 activates Notch in neighboring vascular smooth muscle cells (VMSCs) to regulate VSMC phenotype and arterial homeostasis (29–31). Next, we assessed how different FSS magnitudes influenced Jag1 signaling potential by coculturing endothelial cells exposed to FSS with Notch reporter cells. We inhibited Delta signaling using fucose analogs (32) to evaluate the effect of FSS on Jag1-mediated Notch activation. In agreement with our previous data (33), we found that FSS enhanced Jag1-mediated Notch activation, but Notch activity did not change at the different FSS magnitudes (fig. S5). The data suggest that the increased levels of Jag1 at the lower magnitudes of FSS do not lead to enhanced Notch signal activation, indicating an alternative Jag1 function in endothelial cells.

FSS is sensed by mechanoreceptors that activate downstream signaling to elicit cellular responses (1, 4, 5). We next evaluated the involvement of Jag1 in FSS signaling. We silenced Jag1 using siRNA and assessed the activity of FSS-responsive kinases in endothelial cells (Fig. 1G). The phosphorylation levels of VEGFR2 were reduced in static and flow conditions upon silencing Jag1 (Fig. 1H). Jag1 silencing also decreased the phosphorylation levels of ERK kinase induced by FSS (Fig. 1I) but caused no significant changes in the phosphorylation or total expression levels of AKT (fig. S6).

Mechanical perturbation of Jag1 activates VEGFR2 signaling

Since depletion of Jag1 decreased kinase activity, we next examined if Jag1-mediated kinase activity could be affected by direct physical stimulation of Jag1. To this end, we applied tensional force on Jag1 using 1 µm paramagnetic beads coated with an antibody that recognizes the extracellular domain of Jag1 (J1ECD ab) (Fig. 2A). A similar system has been used to evaluate the mechanosensitivity of proteins involved in FSS signaling (34, 35). Antibody validation using Jag1 wild-type and knockout cells is presented in fig. S7. As additional controls, we included beads coated with an antibody against the extracellular domain of Notch (NECD ab) or beads coated with recombinant Notch extracellular domain (rNECD) or recombinant IgG (rIgG). We exposed HUVECs to the beads for 15 minutes, followed by another 15 minutes of magnetic force field exposure. VEGFR2 activation was increased in endothelial cells

exposed to J1ECD ab-coated beads but not in those exposed to NECD ab-, rNECD-, or rIgG-coated beads (Fig. 2B). Exposing cells to the beads without the magnetic field was sufficient to induce VEGFR2 phosphorylation, but exposing cells to soluble antibodies did not induce VEGFR2 activation, indicating that a physical component is needed for Jag1-induced VEGFR2 activation (Fig. 2C). To further confirm the involvement of Jag1 in VEGFR2 activation, we silenced Jag1 in the endothelial cells. siRNA-mediated Jag1 knockdown prevented VEGFR2 phosphorylation by the J1ECD ab-coated beads (Fig. 2D). While rNECD-coated beads were expected to interact and stimulate Jag1, exposing cells to these beads for 30 minutes was insufficient to produce a detectable increase in VEGFR2 phosphorylation (Fig. 2, B and C). In contrast, when cells were plated over immobilized rNECD peptides for 6 hours (Fig. 2E), we detected increased average phosphorylation levels of VEGFR2 (Fig. 2F) and ERK (Fig. 2G). This is in line with previous reports of recombinant Jag1-coated beads being able to activate Notch after hours of exposure (36–38), in part due to the low affinity of the interaction between Jag1 and Notch compared to that of monoclonal antibodies.

Jag1-mediated signaling is independent of canonical Notch activity

To assess if Jag1-induced VEGFR2 activation required Notch activity, we treated endothelial cells with Notch inhibitors. The γ-secretase inhibitor DAPT was used to prevent Notch cleavage and consequently inhibit canonical (39) and non-canonical cortical Notch activation (16). The more recent inhibitor, CB-103, was used to inhibit Notch transcriptional activation (40). We cultured the cells in the presence of the inhibitors for 24 hours before performing the bead assay to ensure efficient Notch inhibition. Neither inhibition of Notch cleavage nor transcriptional activity prevented Jag1-induced VEGFR2 activation (Fig. 3A). Since canonical Notch activity requires cell-cell contact, seeding the cells at lower confluences reduces Notch activity. We further demonstrated that lowering the confluence of the cultures did not decrease VEGFR2 activation (Fig. 3B). Taken together, the data indicates that Jag1-mediated VEGFR2 activation is independent of canonical or cortical Notch activity.

Jag1-mediated signaling requires Src activation

We next assessed if direct interaction between Jag1 and VEGFR2 was needed to induce VEGFR2 phosphorylation. Jag1 and VEGFR2 did not interact in co-immunoprecipitation assays (Co-IP) (Fig. 3C). It is known that VEGFR2 is activated by the VEGFR2/PECAM/VE-Cadherin (35) and PlexinD1/NRP1 (34) mechanosensitive complexes. To understand if proteins involved in these mechanosignaling complexes were relevant for Jag1-mediated VEGFR2 activation, we used the COS-7 cell line, which lacks the proteins of these FSS junctional complex sensors (34, 35). To our surprise, VEGFR2 was activated by J1ECD ab-coated beads in the absence of any of the other proteins in the complex (Fig. 3D), indicating an alternative mode of VEGFR2 activation. Jag1 signaling has been shown to intersect with Src kinase signaling (41–43), and Src has been shown to operate both downstream and upstream of VEGFR2 (8, 44, 45). Next, we analyzed Src kinase activity in the COS-7 cells treated with the J1ECD ab-coated beads. Jag1 stimulation induced Src and VEGFR2 activity without any other protein of the mechanosensory complexes. Furthermore, Jag1 stimulation induced Src activation even in the absence of VEGFR2 (Fig. 3D), indicating that Src acts upstream of VEGFR2. We found that Src co-immunoprecipitated with Jag1, indicating a potential interaction (Fig. 3E). To

test if Src activity was necessary for VEGFR2 phosphorylation, we stimulated endothelial cells with J1ECD ab-coated beads in the presence and absence of the Src inhibitor Saracatinib. Inhibition of Src prevented VEGFR2 phosphorylation, demonstrating that Jag1-mediated VEGFR2 activation required Src activity (Fig. 3F).

Jag1b KO zebrafish embryos have cardiac edema and decreased ERK activation

VEGFR2, ERK and Src play important roles in cardiovascular development, and zebrafish embryos demonstrate cardiotoxicity after VEGFR2, ERK inhibition, with pericardial edema being one of the established phenotypes (46–48). Our data indicates that Jag1 is required for kinase activity in response to FSS (Fig. 1, G to I) and that direct mechanical stimulation of Jag1 induces kinase activity (Fig. 2). To test if Jag1 affected kinase signaling in vivo, we generated Jag1 knock out (KO) zebrafish (Danio rerio). Zebrafish express two forms of Jag1: jag1a and jag1b. Whereas the extracellular and intracellular domains of jag1b show high similarity to human Jag1, the intracellular domain of jag1a only has 30% similarity with substantial variations in the PDZ-binding motifs (PDZBM) that mediate protein-protein interactions (fig. S8). Double jag1KO gave rise to similar phenotypes previously demonstrated by morpholino-mediated jag1a/b knockdown (49), including defects in the notochord (Fig. 4A). In line with previous reports (50), we did not observe any gross defects in cardiac function as determined by analysis of blood flow activity and heartbeat in the Jag1 KO (Fig. 4, B and C). However, the jag1KO embryos were significantly smaller than the WT counterparts at 3 and 4 dpf (Fig. 4D). Thermal stress increases heart rate and sensitizes zebrafish embryos to cardiac toxicity by kinase inhibitors (51, 52). Intriguingly, we found that jag1bKO but not jag1aKO presented cardiac edema (Fig. 4E), which was more prominent after exposure to thermal stress (Fig. 4, F and G).

We next analyzed kinase activity by western blotting lysates from WT, jag1b heterozygous, and jag1bKO zebrafish embryos. The VEGFR2 antibody was incompatible with zebrafish, but ERK activity was significantly reduced in the heterozygote and jag1bKO compared to WT embryos (Fig. 4H). Since both canonical and non-canonical Jag1 signaling has been shown to affect ERK activity (53, 54), we crossed the Jag1bKO fish with the tg(TP1:H2B-mCherry) Notch reporter line (55) to analyze Notch activity. We did not observe any significant changes in Notch signaling activity upon deletion of jag1b (Fig. 4I), measured by the fluorescence reporter intensity in the heart (Fig. 4J) or in the whole fish (Fig. 4K). This further suggests that Jag1 plays a non-canonical role in regulating the activity of mechanosensitive kinases in the cardiovascular system.

DISCUSSION

Our data shows that Jag1 is responsive to variations in FSS magnitude, with peak expression occurring at lower FSS magnitudes. This aligns with the observed high expression of Jag1 in atheroprone regions characterized by low oscillatory FSS (26). Such selective sensitivity could explain the tissue- and context-specific disease manifestations seen in patients with Jag1 mutations (56). We observed that Jag1 re-localizes in response to FSS, first into subcellular clusters (33) and later polarized downstream of the flow direction. Notch has previously been shown to also polarize in the direction of flow (24). Since cis-interactions with Jag1 inhibit Notch activation (57), our data could help explain the contrasting effects of Notch and Jag1 in atherosclerosis (24, 26). The pro-atherogenic role of Jag1 may be related in part to cis-inhibition of Notch by Jag1 in regions of low oscillatory flow or to Notch-independent functions in kinase signaling. Our results demonstrate uncoupling of Jag1 and Notch expression patterns and activity in line with their different roles in various vascular processes.

Jag1 deletion reduces FSS-induced activation of VEGFR2 and ERK. While we found Jag1 to be a positive regulator of ERK activity, Cuervo et al., 2023 (58) showed Notch having an opposite effect on ERK activity. Our data also shows that direct physical stimulation of Jag1 activates VEGFR2. VEGFR2 is a key regulator of angiogenesis, and Jag1 is also a potent pro-angiogenic regulator and is thought to antagonize Dll4-mediated Notch activity. Based on our findings, Jag1 may also directly enhance VEGFR2's activity. Further studies are needed to evaluate if this is the case.

Mechanical perturbation of Jag1 induces Src activity which in turn is required for Jag1-mediated VEGFR2 activation. Even though Jag1-mediated VEGFR2 activation seems to be effectuated through Src, the detailed mechanism is still unclear. The soluble cleaved extracellular domain of Jag1 has been shown to activate Src in the vasculature by modulating both canonical and non-canonical Notch signaling pathways (41). However, Jag1-mediated VEGFR2 activation does not require Notch activity. We show that VEGFR2 can be activated in the presence of the γ-secretase inhibitor DAPT that inhibits both canonical and non-canonical Notch activity (16, 39). Both Jag1 and Src have a PDZBM in their structure, which could mediate their interaction through PDZ domain-containing scaffold proteins regulating Src activity. One possible protein that could serve this purpose is Afadin. Both Src (59) and Jag1 (60) bind the junctional scaffolding protein through their PDZBM. Afadin is known to regulate the localization and activity of Src and it is also known to be phosphorylated by Src. PDZ domains were recently suggested to form mechanosensitive catch bonds with mechanical load regulating the selectivity of PDZ-peptide interactions (61). FSS-induced modulation of Afadin, Jag1, and Src interactions may promote Src activity and VEGFR2 phosphorylation.

ERK plays an essential role in the morphogenesis of the outflow tract in zebrafish (62) and pericardial edema is one of the main effects of ERK inhibition (46–48). While both Notch (63, 64) and Jag1 (53, 54) have been previously shown to influence ERK activation in vitro, we show that Jag1 deletion attenuates ERK activity and promotes pericardial edema in vivo in the absence of detectable change in Notch activation. Taken together our data describes a new non-canonical Notch-independent role of Jag1 in endothelial mechanotransduction that may contribute to cardiovascular morphogenesis and disease progression.

MATERIALS AND METHODS

Cell culture

Pooled human umbilical vein endothelial cells (HUVEC) (PromoCell) were cultured in Endothelial Cell Growth Medium 2 (PromoCell) completed with Endothelial Cell Growth Medium 2 SupplementMix (PromoCell). Human Aortic Endothelial Cells (HAoEC) (PromoCell) were cultured in Endothelial Cell Growth Medium MV (PromoCell) completed with Growth Medium MV SupplementMix (PromoCell). Thawing and expansion of primary endothelial cells were executed according to the PromoCell Instruction Manual, and all experiments, unless stated otherwise, were done using fully confluent cells at passages 5-6. COS-7 cells were cultured in DMEM (Sigma) supplemented with 10% FBS, 100 U/ml penicillin, and 100 µg/ml streptomycin. All cells were seeded and expanded on tissue culture polystyrene (TCPS) plates and maintained at 37 °C, 5% CO2.

Experimental animals

Jagged1a (sa11248) zebrafish embryos were purchased from the Karlsruhe Institute of Technology (KIT.) Jagged1b (b1105) (65) was generously provided by the Crump Lab at the University of Southern California, Keck School of Medicine. All the experiments were carried out at Turku Bioscience Center Zebrafish Core under license ESAVI/31414/2020 and ESAVI/44584/2023 granted by The Regional Administration Office of Southern Finland. Jag1a +/-; Jag1b +/- strain and TP1:H2B-mCherry; Jag1b+/- strain were created in Turku by crossing Jag1b +/- together with Jag1a +/- strain or with tg(TP1:H2B-mCherry) strain (55) generously provided by the Ninov Lab at the Center for Regenerative Therapies Dresden (CRTD) at TUD Dresden University of Technology. Embryos used for imaging were kept in E3 media (5 mM NaCl, 0.17 mM KCl, 0.33 mM CaCl2, 0.33 mM MgSO4) supplemented with 30 mg/ml of 1-phenyl 2-thiourea (PTU) either in 28.5°C or in 33°C. Heart rate and blood flow videos were taken 2-, 3- and 4-days post fertilization (dpf) at room temperature with a frame rate of 42 frames per second (fps) using Zeiss AxioZoom V.16 stereomicroscope with 1.0x Plan ApoZ (NA 0.125) objective and Hamamatsu sCMOS ORCA-Flash4.0 LT. The same microscope and camera were used to image embryos carrying tg(*TP1:H2B-mCherry*) reporter. During the imaging, embryos were anesthetized with Tricaine 160 mg/ml. To match the developmental stages of embryos kept at different temperatures, the developmental stages were calculated as described in (66). Heart rate, blood flow activity and pericardial area were measured by using DanioScope software from Noldus. Fish length and Notch activity were measured using ImageJ FIJI image analysis software. For Western blot, embryos were genotyped and then pooled accordingly. Embryos were lysed with 3x Laemmli buffer (30 % Glycerol, 3 % SDS, 0.1875 M Tris-HCl pH 6.8, 0.015 % bromophenol blue, 3% β-mercaptoethanol) and boiled 15 minutes at 95°C.

For genotyping, the genomic DNA was extracted from each embryo via alkaline lysis using 50 mM NaOH and boiling the samples for 15 minutes at 95°C. Samples were vortexed every 5 minutes and at the end centrifuged 5 minutes, 14 000 relative centrifugal force (rcf) at 4°C. DreamTaq DNA polymerase (Thermo Scientific) was used in gene amplification according to the manufacturer's instructions followed by restriction enzyme treatment. BsmAI (New England Biolabs) was used for jag1a genotyping and BseGI (BtsCI) (Thermo Fisher Scientific) for jag1b genotyping. Samples were analyzed from 2.5% Agarose gel.

Primers

Gene	Forward primer	Reverse primer
Jag1a (sa11248)	GACCAGTGTTTATCCATTCCCC	CACTTTGACCATCCGCTCTCA
Jag1b (b1105)	GTACCAAATCCGGGTGACCT	GTGGCTTTTTGGGTCATTATCA

Jag1a	Jag1b
Mutation adds BsmAI site	Mutation destroys BseGI site
+/+: 514, 106	+/+: 134, 72
+/-: 514, 333, 181, 106	+/-: 206, 134, 72
-/-: 333, 181, 106	-/-: 206

Shear stress experiments

For imaging experiments, HUVECs and HAoECs were seeded into 6-channel slides (Ibidi, 80606 coated with 100 µg / ml Bovine Type I Collagen solution (Advanced BioMatrix Inc., 5010) with 1 x 10^5 cells added per channel. Media was changed twice a day. Cells were allowed to attach and form a monolayer overnight, after which they were subjected to shear stress or maintained as static control. Flow over cells was achieved by assembling a perfusion set consisting of the 6-channel slide connected to a glass bottle with 25 ml of respective culture media via 1.6 mm inner diameter silicone tubing (ibidi, 10842) and attached to a REGLO Analog peristaltic pump (Ismatec) via three-stop-tubing, creating a loop for media recirculation during the experiment. Utilizing a three-port screw cap on the glass bottle, a 22 µm pore diameter syringe filter was attached to the bottle to allow air pressure equilibration in the system. At the start of a shear stress experiment, the flow rate of the system was increased in a step-wise manner over one hour by changing the pump rpm, starting from 0 rpm, followed by 22, 66, and 99 rpm steps, 99 rpm equaling 1.4 Pa of laminar and continuous FSS. Cells were exposed to flow for 24 to 25 hours at 1.4 Pa. The media was preconditioned to the temperature, humidity and CO2 conditions of the experiment by putting it in a glass bottle inside the incubator overnight before the assembly of the perfusion set.

For gene expression experiments, HUVECs were seeded at 10^6 cells/ml into collagen IV-coated 1-channel slides for gene expression analysis and 6-channel slides (Ibidi, 80172) for immunocytochemistry or the reporter cell assay. After one day of culture, the endothelial cells were subjected to FSS using the Ibidi pump system (Ibidi) or kept in culture as a static control. The standard perfusion sets were adjusted to gain a stable flow speed and pressure. Resistance tubing (0.5 mm inner diameter) was added after the channel slides to stabilize the fluctuations in flow speed. The cells were exposed to 0.5, 1, or 2 Pa FSS for 24 hours. Flow speeds were constantly measured to ensure correct flow speed (ME2PXL flow sensor, Transonic Systems Inc.). Flow was laminar and continuous except when the effect of pulsatile flow was evaluated (fig. S4).

For protein and post-translational modification analysis, cells were seeded in 6-well plates and grown to full confluency. Before flowing, in the beginning of the experiment, the media was changed to ensure an initial volume of 3mL per well and the plate was placed on a CO2-resistant orbital shaker. A computational fluid dynamics simulation was performed as previously described (28). The simulation values were used to

select the speed of the orbital shaker, and in all cases, a non-flowed plate (Static) was used as a control. Unless stated otherwise, plates were collected after 24 hours and placed on ice, and approximately 64% of the outermost area of the well was collected.

Immunocytochemistry

After the shear stress experiment, cells in the 6-channel Ibidi slides were washed two to three times with 37°C modified (without $CaCl_2$, $MgCl_2$) Dulbecco's Phosphate-Buffered Saline (DPBS) and fixed in 37°C 4% paraformaldehyde in DPBS for 10 minutes, followed by another three washes with DPBS modified. Slides with fixed cells were stored for up to 16 days at a temperature of 4°C in the dark. Cells were permeabilized in 0.2% Triton X-100 in DPBS for 5 and 10 minutes at room temperature (RT), after which they were washed once with modified DPBS. Blocking of the cells was done by incubation in 1% BSA in PBS at RT for 30 minutes, followed by three washes with modified DPBS. Cells were incubated with Jagged1 (Cell Signaling Technology; 2620; 1:100) and CD31 (Invitrogen; 37-0700; 1:100) monoclonal primary antibodies in the solution of 3% BSA and 0.05% Triton X-100 in DPBS overnight at 4°C in the dark. Cell was washed three times with modified DPBS and incubated with secondary antibodies (Donkey anti-Mouse IgG Alexa Fluor 488; A-21202; 1:500, Goat anti-Rabbit IgG Alexa Fluor 555; A-21428, 1:500) and DAPI (Sigma-Aldrich, D9542) in 3% BSA and 0.05% Triton X-100 in PBS for 1 hour at RT in the dark. The staining solution was removed, and cells were washed three times in RT-modified DPBS and imaged with the channels filled with PBS.

Imaging was conducted with a Zeiss LSM 880 Airyscan confocal with an Axio Observer.Z1 microscope using ZEN 2.3 SP1 black edition acquisition software. The objective used was 63x Zeiss C Plan-Apochromat Oil DIC M27 with 1.4 aperture. The pinhole was set to give the same optical section thickness for all channels. DAPI was excited with a diode at a wavelength of 405 nm and acquired at an emission window of 410-514 nm with a PMT with the pinhole set to 3.85 airy units (AU). Alexa Fluor 488 was excited with Argon laser at a wavelength of 488 nm and acquired at an emission window of 490 – 579 nm with GaAsP detector with pinhole set to 3.10 AU. Alexa Fluor 555 was excited with HeNe laser at a wavelength of 543 and acquired at an emission window of 556 – 648 with a cooled PMT with the pinhole set to 2.69 AU. Channels were acquired sequentially and with unidirectional scanning, 4 times line averaging, and pixel dwell time of 1.02 µs at a bit depth of 8 bits. All images were acquired with 1x1 binning, and the XYZ pixel dimensions varied across experiments within 85 – 132 nm in X and Y and 632-1090 nm in Z.

Co-immunoprecipitations and Western blots

Cells were collected in lysis buffer (50 mM Tris, pH 7.5, 150 mM NaCl, 1% Triton X-100, 0.1% SDS) with protease (Complete™ Protease Inhibitor Cocktail, Merck) and phosphatase inhibitor cocktail (Pierce™ Phosphatase Inhibitor Mini Tablets, ThermoFisher). Lysates were collected and kept on ice during sonication before being centrifuged for 10 minutes at 14 000 rcf at 4°C. The supernatant was used for the input control and the subsequent processing steps. Beads were washed five times with washing buffer (50 mM Tris-HCl (pH 7.5); 250 mM NaCl; 0,1% NP-40) before use. Lysates were pre-cleared using 5 µL of washed beads per sample. After pre-clearing, samples were incubated overnight at 4 °C with antibody (Jag1 28H8 1:50, VEGFR2 55B11 1:100 or IgG (DA1E); all from Cell Signaling Technologies (CST)). Samples were then incubated at RT for 1.5 hours with 16.5 µl of washed beads per sample.

Finally, beads were washed three times with a washing buffer and, one final time, with MilliQH_2O before being diluted in Laemmli sample buffer for western blotting.

Proteins were separated by SDS-PAGE and transferred to a Protran nitrocellulose membrane (GE Healthcare Life Sciences) using a wet transfer apparatus (Amersham Bioscience). The membranes were blocked with 5% nonfat dry milk in TBS at RT for 0.5- 1 hour. Primary antibody incubation was done overnight at 4 °C in constant agitation. Membranes were then incubated in secondary antibody for 1 hour at RT (1:10000). Proteins were acquired using an iBright Imaging System (ThermoFisher) after incubation with SuperSignal West Pico PLUS Enhanced chemiluminescence substrate (ThermoFisher). The following antibodies were used: Jag1 28H8, VEGFR2 55B11, phospho-Tyr1175 VEGFR2 2478, p44/42 MAPK (Erk1/2) 9102S, phospho-Y204-Erk1 / phospho-Y187-Erk2 5726S, Akt 9272, phospho-Ser473 Akt 4060S, CD31 (PECAM-1) D8V9E, VE-Cadherin D87F2, Src 2108S and Phospho-Src Family (Tyr416) D49G4 all purchased from CST. HSC70 (ADI-SPA-815-D, Enzo) or Revert 700 Total Protein Stain (LI-COR) was used for loading control. The densitometry level were obtained using the image analysis software ImageJ FIJI.

Magnetic bead experiments

Experiments were performed using 24-well plates. 1.0 µm Protein A/G Magnetic Beads (ThermoFisher) were washed with TBS and functionalized for 1.5 hour at RT with antibodies (Jag1 1C4, IgG DA1E from CST; Notch 2 ECD MA5-24274 from ThermoFisher) or recombinant peptides (Recombinant Human Notch-1 Fc chimera protein and IgG-Fc chimera protein from R&D systems). Cells were incubated with beads at 37°C, 5% CO_2 for 15 minutes before exposure to a magnetic field using permanent magnets for another 15 minutes or were incubated for 30 minutes before being lysed and collected for western-blot analysis.

Pharmacological inhibitions

HUVECs were treated with the γ-secretase inhibitor 1N-[N-(3,5-difluorophenacetyl)-l-alanyl]-S-phenylglycine t-butyl ester (DAPT) to inhibit Notch cleavage or CB-103 to inhibit Notch-induced transcriptional activation, both at 25 µM. To inhibit Src, HUVECs were incubated with the inhibitor Saracatinib at 10 µM. All inhibitors were added in fresh media, 24 hours before experiments were performed. Inhibitors were dissolved in DMSO, and control experiments were performed in the presence of the same amount of DMSO as vehicle control.

Gene expression

RNA was isolated with the Qiagen RNeasy kit. The β-mercaptoethanol – RLT buffer mixture was directly added to the cells in the 1-channel slides. The synthesis of cDNA was performed with M-MLV reverse transcriptase (Invitrogen). For six reference genes tested GAPDH was the most stably expressed, as analyzed with GeNorm130. The PCR protocol consisted of 3 minutes at 95°C, followed by 40 cycles of 20 s at 95°C, 20 s at 60°C and 30 s at 72°C. Data were analyzed using the ΔΔCt method. The primers used can be found in Table S1.

Notch reporter assay

HEK293T cells were transfected with 12xCSL-luciferase223 or GFP as a transfection control using polyethyleneimine (PEI), 1 mg/ml. For transfection, DNA and PEI were

mixed at 1:2 weight ratio in plain medium. After 5-minute incubation, the DNA-PEI mixture was added to the HEK293T cell culture. Next day, the cells were washed with PBS and used for the reporter assay. After flow experiments, endothelial cells were washed twice with PBS. Transfected HEK293T cells were seeded directly on top of endothelial cells (10^6 cells/ml, 50 µl/channel) and cultured in EGM2 medium for 24 hours. In half of the channels (3), the cells were cocultured in the presence of 50 µM 6-alkynyl-fucose (Peptides International). In the other channels, the cells were cultured in an equal amount of DMSO as a control. Notch activity was assessed by measuring luciferase activity from lysed cells using Luciferase Assay from Promega. Biotek Synergy plate reader was used in signal detection.

Statistical analysis

P-values were obtained after parametric tests were conducted. For two group comparisons a two-tailed Student's T-test was performed. When three or more comparisons or more than one independent variable were present, two-way ANOVA were performed to assess main effects, with post-hoc testing. Dunnet's post-hoc test was used when groups were compared with normalizing control. Tukey's post-hoc test was used when all groups where compare with each other. Bonferroni correction was performed when four or more preselected comparisons against controls were made. For four or less comparisons Fishers LSD test was used as the post-hoc test. All error bars represent the SEM. The graphs were made using an established color-blind friendly palette (67). Graph and statistical analysis were performed using the statistical software GraphPad Prism 10.

Supplementary Materials

fig. S1. FSS-induced polarization of Jag1 in HUVEC.

fig. S2. Expression of Notch-related genes in response to different magnitudes of FSS.

fig. S3. FSS-induced Jag1 protein expression over time.

fig. S4. Gene expression of Notch-related genes in response to different flow patterns.

fig. S5. Jag1-Notch transactivation potential in static and shear-stressed HUVECs.

fig. S6. AKT expression and activation was unaffected by Jag1 silencing using siRNAs.

fig. S7. Validation of the antibody targeting the extracellular domain of Jag1.

fig. S8. Sequence alignment of the N-terminal region of different Jag1 orthologs.

Table S1. Primer list.

REFERENCES AND NOTES

1. N. Baeyens, C. Bandyopadhyay, B. G. Coon, S. Yun, M. A. Schwartz, Endothelial fluid shear stress sensing in vascular health and disease. *J. Clin. Invest.* **126**, 821–828 (2016).

2. E. Roux, P. Bougaran, P. Dufourcq, T. Couffinhal, Fluid Shear Stress Sensing by the Endothelial Layer. *Front. Physiol.* **11**, 861 (2020).

3. R. Li, K. I. Baek, C.-C. Chang, B. Zhou, T. K. Hsiai, Mechanosensitive Pathways Involved in Cardiovascular Development and Homeostasis in Zebrafish. *J. Vasc. Res.* **56**, 273–283 (2019).

4. C. Souilhol, J. Serbanovic-Canic, M. Fragiadaki, T. J. Chico, V. Ridger, H. Roddie, P. C. Evans, Endothelial responses to shear stress in atherosclerosis: a novel role for developmental genes. *Nat. Rev. Cardiol.* **17**, 52–63 (2020).

5. I. A. Tamargo, K. I. Baek, Y. Kim, C. Park, H. Jo, Flow-induced reprogramming of endothelial cells in atherosclerosis. *Nat. Rev. Cardiol.* **20**, 738–753 (2023).

6. E. E. van Haaften, C. V. C. Bouten, N. A. Kurniawan, Vascular Mechanobiology: Towards Control of In Situ Regeneration. *Cells* **6**, 19 (2017).

7. K. Katoh, Effects of Mechanical Stress on Endothelial Cells In Situ and In Vitro. *Int. J. Mol. Sci.* **24**, 16518 (2023).

8. C. Aitken, V. Mehta, M. A. Schwartz, E. Tzima, Mechanisms of endothelial flow sensing. *Nat. Cardiovasc. Res.* **2**, 517–529 (2023).

9. S. G. Rahaman, M. Mahanty, P. Mukherjee, B. Dutta, S. O. Rahaman, Mechanosensing and Mechanosignal Transduction in Atherosclerosis. *Curr. Atheroscler. Rep.* **25**, 711–721 (2023).

10. K. Tanaka, D. Joshi, S. Timalsina, M. A. Schwartz, Early events in endothelial flow sensing. *Cytoskeleton* **78**, 217–231 (2021).

11. S. Cavallero, A. M. Blázquez-Medela, S. Satta, T. K. Hsiai, Endothelial mechanotransduction in cardiovascular development and regeneration: emerging approaches and animal models. *Curr. Top. Membr.* **87**, 131–151 (2021).

12. M. Fernández-Chacón, I. García-González, S. Mühleder, R. Benedito, Role of Notch in endothelial biology. *Angiogenesis* **24**, 237–250 (2021).

13. D. MacGrogan, J. Münch, J. L. de la Pompa, Notch and interacting signalling pathways in cardiac development, disease, and regeneration. *Nat. Rev. Cardiol.* **15**, 685–704 (2018).

14. J. Grego-Bessa, L. Luna-Zurita, G. del Monte, V. Bolós, P. Melgar, A. Arandilla, A. N. Garratt, H. Zang, Y. Mukouyama, H. Chen, W. Shou, E. Ballestar, M. Esteller, A. Rojas, J. M. Pérez-Pomares, J. L. de la Pompa, Notch Signaling Is Essential for Ventricular Chamber Development. *Dev. Cell* **12**, 415–429 (2007).

15. S. S. Hasan, A. Fischer, Notch Signaling in the Vasculature: Angiogenesis and Angiocrine Functions. *Cold Spring Harb. Perspect. Med.*, a041166 (2022).

16. W. J. Polacheck, M. L. Kutys, J. Yang, J. Eyckmans, Y. Wu, H. Vasavada, K. K. Hirschi, C. S. Chen, A non-canonical Notch complex regulates adherens junctions and vascular barrier function. *Nature* **552**, 258–262 (2017).

17. R. Priya, S. Allanki, A. Gentile, S. Mansingh, V. Uribe, H.-M. Maischein, D. Y. R. Stainier, Tension heterogeneity directs form and fate to pattern the myocardial wall. *Nature* **588**, 130–134 (2020).

18. D.-Y. Tian, X.-R. Jin, X. Zeng, Y. Wang, Notch Signaling in Endothelial Cells: Is It the Therapeutic Target for Vascular Neointimal Hyperplasia? *Int. J. Mol. Sci.* **18**, 1615 (2017).

19. J. Falo-Sanjuan, S. J. Bray, Decoding the Notch signal. *Dev. Growth Differ.* **62**, 4–14 (2020).

20. O. M. J. A. Stassen, T. Ristori, C. M. Sahlgren, Notch in mechanotransduction – from molecular mechanosensitivity to tissue mechanostasis. *J. Cell Sci.* **133**, jcs250738 (2020).

21. F. Suarez Rodriguez, S. Sanlidag, C. Sahlgren, Mechanical regulation of the Notch signaling pathway. *Curr. Opin. Cell Biol.* **85**, 102244 (2023).

22. V. Tsata, D. Beis, In Full Force. Mechanotransduction and Morphogenesis during Homeostasis and Tissue Regeneration. *J. Cardiovasc. Dev. Dis.* **7**, 40 (2020).

23. J. S. Fang, B. G. Coon, N. Gillis, Z. Chen, J. Qiu, T. W. Chittenden, J. M. Burt, M. A. Schwartz, K. K. Hirschi, Shear-induced Notch-Cx37-p27 axis arrests endothelial cell cycle to enable arterial specification. *Nat. Commun.* **8**, 2149 (2017).

24. J. J. Mack, T. S. Mosqueiro, B. J. Archer, W. M. Jones, H. Sunshine, G. C. Faas, A. Briot, R. L. Aragón, T. Su, M. C. Romay, A. I. McDonald, C.-H. Kuo, C. O. Lizama, T. F. Lane, A. C. Zovein, Y. Fang, E. J. Tarling, T. Q. de Aguiar Vallim, M. Navab, A. M. Fogelman, L. S. Bouchard, M. L. Iruela-Arispe, NOTCH1 is a mechanosensor in adult arteries. *Nat. Commun.* **8**, 1620 (2017).

25. C. L. Karthika, V. Venugopal, B. J. Sreelakshmi, S. Krithika, J. M. Thomas, M. Abraham, C. C. Kartha, A. Rajavelu, S. Sumi, Oscillatory shear stress modulates Notch-mediated endothelial mesenchymal plasticity in cerebral arteriovenous malformations. *Cell. Mol. Biol. Lett.* **28**, 22 (2023).

26. C. Souilhol, B. Tardajos Ayllon, X. Li, M. R. Diagbouga, Z. Zhou, L. Canham, H. Roddie, D. Pirri, E. V. Chambers, M. J. Dunning, M. Ariaans, J. Li, Y. Fang, H. F. Jørgensen, M. Simons, R. Krams, J. Waltenberger, M. Fragiadaki, V. Ridger, S. De Val, S. E. Francis, T. J. Chico, J. Serbanovic-Canic, P. C. Evans, JAG1-NOTCH4 mechanosensing drives atherosclerosis. *Sci. Adv.* **8**, eabo7958 (2022).

27. B. J. Sreelakshmi, C. L. Karthika, S. Ahalya, S. R. Kalpana, C. C. Kartha, S. Sumi, Mechanoresponsive ETS1 causes endothelial dysfunction and arterialization in varicose veins *via* NOTCH4/DLL4 signaling. *Eur. J. Cell Biol.* **103**, 151420 (2024).

28. R. C. H. Driessen, F. Zhao, S. Hofmann, C. Bouten, C. Sahlgren, O. Stassen, Computational Characterization of the Dish-In-A-Dish, A High Yield Culture Platform for Endothelial Shear Stress Studies on the Orbital Shaker. *Micromachines* **11**, 552 (2020).

29. N. C. A. van Engeland, F. Suarez Rodriguez, A. Rivero-Müller, T. Ristori, C. L. Duran, O. M. J. A. Stassen, D. Antfolk, R. C. H. Driessen, S. Ruohonen, S. T. Ruohonen, S. Nuutinen, E. Savontaus, S. Loerakker, K. J. Bayless, M. Sjöqvist, C. V. C. Bouten, J. E. Eriksson, C. M. Sahlgren, Vimentin regulates Notch signaling strength and arterial remodeling in response to hemodynamic stress. *Sci. Rep.* **9**, 12415 (2019).

30. Y. Zhang, M. Hernandez, J. Gower, N. Winicki, X. Morataya, S. Alvarez, J. X.-J. Yuan, J. Shyy, P. A. Thistlethwaite, JAGGED-NOTCH3 signaling in vascular remodeling in pulmonary arterial hypertension. *Sci. Transl. Med.* **14**, eabl5471 (2022).

31. R. M. Breikaa, K. Denman, Y. Ueyama, P. E. McCallinhart, A. Q. Khan, G. Agarwal, A. J. Trask, V. Garg, B. Lilly, Loss of *Jagged1* in mature endothelial cells causes vascular dysfunction with alterations in smooth muscle phenotypes. *Vascul. Pharmacol.* **145**, 107087 (2022).

32. M. Schneider, V. Kumar, L. U. Nordstrøm, L. Feng, H. Takeuchi, H. Hao, V. C. Luca, K. C. Garcia, P. Stanley, P. Wu, R. S. Haltiwanger, Inhibition of Delta-induced Notch signaling using fucose analogs. *Nat. Chem. Biol.* **14**, 65–71 (2018).

33. R. C. H. Driessen, O. M. J. A. Stassen, M. Sjöqvist, F. Suarez Rodriguez, J. Grolleman, C. V. C. Bouten, C. M. Sahlgren, Shear stress induces expression, intracellular reorganization and enhanced Notch activation potential of Jagged1. *Integr. Biol.* **10**, 719–726 (2018).

34. V. Mehta, K.-L. Pang, D. Rozbesky, K. Nather, A. Keen, D. Lachowski, Y. Kong, D. Karia, M. Ameismeier, J. Huang, Y. Fang, A. del Rio Hernandez, J. S. Reader, E. Yvonne Jones, E. Tzima, The Guidance Receptor Plexin D1 Moonlights as an Endothelial Mechanosensor. *Nature* **578**, 290–295 (2020).

35. E. Tzima, M. Irani-Tehrani, W. B. Kiosses, E. Dejana, D. A. Schultz, B. Engelhardt, G. Cao, H. DeLisser, M. A. Schwartz, A mechanosensory complex that mediates the endothelial cell response to fluid shear stress. *Nature* **437**, 426–431 (2005).

36. J. De La Croix Ndong, Y. Stephenson, M. E. Davis, A. J. Garc í a, S. Goudy, Controlled JAGGED1 delivery induces human embryonic palate mesenchymal cells to form osteoblasts. *J. Biomed. Mater. Res. A* **106**, 552–560 (2018).

37. F. Zhu, M. T. Sweetwyne, K. D. Hankenson, PKCδ Is Required for Jagged-1 Induction of Human Mesenchymal Stem Cell Osteogenic Differentiation. *Stem Cells* **31**, 1181–1192 (2013).

38. K. Zohorsky, S. Lin, K. Mequanint, Immobilization of Jagged1 Enhances Vascular Smooth Muscle Cells Maturation by Activating the Notch Pathway. *Cells* **10**, 2089 (2021).

39. C. Song, J. Zhang, C. Xu, M. Gao, N. Li, Q. Geng, The critical role of γ-secretase and its inhibitors in cancer and cancer therapeutics. *Int. J. Biol. Sci.* **19**, 5089–5103 (2023).

40. R. Lehal, J. Zaric, M. Vigolo, C. Urech, V. Frismantas, N. Zangger, L. Cao, A. Berger, I. Chicote, S. Loubéry, S. H. Choi, U. Koch, S. C. Blacklow, H. G. Palmer, B. Bornhauser, M. González-Gaitán, Y. Arsenijevic, V. Zoete, J. C. Aster, J.-P. Bourquin, F. Radtke, Pharmacological disruption of the Notch transcription factor complex. *Proc. Natl. Acad. Sci. U. S. A.* **117**, 16292–16301 (2020).

41. K. Miloudi, M. Oubaha, C. Ménard, A. Dejda, V. Guber, G. Cagnone, A. M. Wilson, N. Tétreault, G. Mawambo, F. Binet, R. Chidiac, C. Delisle, M. Buscarlet, A. Cerani, S. Crespo-Garcia, K. Bentley, F. Rezende, J.-S. Joyal, F. A. Mallette, J.-P. Gratton, B. Larrivée, P. Sapieha, NOTCH1 signaling induces pathological vascular permeability in diabetic retinopathy. *Proc. Natl. Acad. Sci. U. S. A.* **116**, 4538–4547 (2019).

42. D. Small, D. Kovalenko, D. Kacer, L. Liaw, M. Landriscina, C. Di Serio, I. Prudovsky, T. Maciag, Soluble Jagged 1 Represses the Function of Its Transmembrane Form to Induce the Formation of the Src-dependent Chord-like Phenotype*. *J. Biol. Chem.* **276**, 32022–32030 (2001).

43. R. Trifonova, D. Small, D. Kacer, D. Kovalenko, V. Kolev, A. Mandinova, R. Soldi, L. Liaw, I. Prudovsky, T. Maciag, The Non-transmembrane Form of Delta1, but Not of Jagged1, Induces Normal Migratory Behavior Accompanied by Fibroblast Growth Factor Receptor 1-dependent Transformation*. *J. Biol. Chem.* **279**, 13285–13288 (2004).

44. Z.-G. Jin, H. Ueba, T. Tanimoto, A. O. Lungu, M. D. Frame, B. C. Berk, Ligand-Independent Activation of Vascular Endothelial Growth Factor Receptor 2 by Fluid Shear Stress Regulates Activation of Endothelial Nitric Oxide Synthase. *Circ. Res.* **93**, 354–363 (2003).

45. B. Miller, M. K. Sewell-Loftin, Mechanoregulation of Vascular Endothelial Growth Factor Receptor 2 in Angiogenesis. *Front. Cardiovasc. Med.* **8**, 804934 (2022).

46. C. Anastasaki, K. A. Rauen, E. E. Patton, Continual low-level MEK inhibition ameliorates cardio-facio-cutaneous phenotypes in zebrafish. *Dis. Model. Mech.* **5**, 546–552 (2012).

47. R. E. Bolcome, J. Chan, Constitutive MEK1 Activation Rescues Anthrax Lethal Toxin-Induced Vascular Effects In Vivo. *Infect. Immun.* **78**, 5043–5053 (2010).

48. C. Ma, Z. Wu, X. Wang, M. Huang, X. Wei, W. Wang, H. Qu, X. Qiaolongbatu, Y. Lou, L. Jing, G. Fan, A systematic comparison of anti-angiogenesis efficacy and cardiotoxicity of receptor tyrosine kinase inhibitors in zebrafish model. *Toxicol. Appl. Pharmacol.* **450**, 116162 (2022).

49. M. Yamamoto, R. Morita, T. Mizoguchi, H. Matsuo, M. Isoda, T. Ishitani, A. B. Chitnis, K. Matsumoto, J. G. Crump, K. Hozumi, S. Yonemura, K. Kawakami, M. Itoh, Mib-Jag1-Notch signalling regulates patterning and structural roles of the notochord by controlling cell-fate decisions. *Dev. Camb. Engl.* **137**, 2527–2537 (2010).

50. K. Lorent, S.-Y. Yeo, T. Oda, S. Chandrasekharappa, A. Chitnis, R. P. Matthews, M. Pack, Inhibition of Jagged-mediated Notch signaling disrupts zebrafish biliary development and generates multi-organ defects compatible with an Alagille syndrome phenocopy. *Development* **131**, 5753–5766 (2004).

51. A.-M. Haapanen-Saaristo, N. Virtanen, E. Tcarenkova, K. Vaparanta, M. Ampuja, E.-R. Vehniäinen, I. Paatero, Heat stress sensitizes zebrafish embryos to neurological and cardiac toxicity. *Biochem. Biophys. Res. Commun.* **733**, 150682 (2024).

52. K. Rayani, E. Lin, C. Craig, M. Lamothe, S. Shafaattalab, M. Gunawan, A. Y. Li, L. Hove-Madsen, G. F. Tibbits, Zebrafish as a model of mammalian cardiac function: Optically mapping the interplay of temperature and rate on voltage and calcium dynamics. *Prog. Biophys. Mol. Biol.* **138**, 69–90 (2018).

53. M. Pelullo, F. Nardozza, S. Zema, R. Quaranta, C. Nicoletti, Z. M. Besharat, M. P. Felli, B. Cerbelli, G. d'Amati, R. Palermo, C. Capalbo, C. Talora, L. Di Marcotullio, G. Giannini, S. Checquolo, I. Screpanti, D. Bellavia, Kras/ADAM17-Dependent Jag1-ICD Reverse Signaling Sustains Colorectal Cancer Progression and Chemoresistance. *Cancer Res.* **79**, 5575–5586 (2019).

54. M. D. Sanna, V. Borgonetti, N. Galeotti, μ Opioid Receptor-Triggered Notch-1 Activation Contributes to Morphine Tolerance: Role of Neuron–Glia Communication. *Mol. Neurobiol.* **57**, 331–345 (2020).

55. N. Ninov, M. Borius, D. Y. R. Stainier, Different levels of Notch signaling regulate quiescence, renewal and differentiation in pancreatic endocrine progenitors. *Development* **139**, 1557–1567 (2012).

56. J. Mašek, E. R. Andersson, Jagged-mediated development and disease: Mechanistic insights and therapeutic implications for Alagille syndrome. *Curr. Opin. Cell Biol.* **86**, 102302 (2024).

57. R. Thambyrajah, M. Maqueda, W. H. Neo, K. Imbach, Y. Guillén, D. Grases, Z. Fadlullah, S. Gambera, F. Matteini, X. Wang, F. J. Calero-Nieto, M. Esteller, M. C. Florian, E. Porta, R. Benedito, B. Göttgens, G. Lacaud, L. Espinosa, A. Bigas, Cis inhibition of NOTCH1 through JAGGED1 sustains embryonic hematopoietic stem cell fate. *Nat. Commun.* **15**, 1604 (2024).

58. H. Cuervo, S. Mühleder, I. García-González, R. Benedito, Notch-mediated cellular interactions between vascular cells. *Curr. Opin. Cell Biol.* **85**, 102254 (2023).

59. G. Radziwill, A. Weiss, J. Heinrich, M. Baumgartner, P. Boisguerin, K. Owada, K. Moelling, Regulation of c-Src by binding to the PDZ domain of AF-6. *EMBO J.* **26**, 2633–2644 (2007).

60. M. Popovic, J. Bella, V. Zlatev, V. Hodnik, G. Anderluh, P. N. Barlow, A. Pintar, S. Pongor, The interaction of Jagged-1 cytoplasmic tail with afadin PDZ domain is local, folding-independent, and tuned by phosphorylation. *J. Mol. Recognit.* **24**, 245–253 (2011).

61. V. T. Vachharajani, M. P. DeJong, A. R. Dunn, PDZ Domains from the Junctional Proteins Afadin and ZO-1 Act as Mechanosensors. *bioRxiv*, 2023.09.24.559210 (2023).

62. M. L. Kelly, A. Astsaturov, J. Rhodes, J. Chernoff, A Pak1/Erk Signaling Module Acts through Gata6 to Regulate Cardiovascular Development in Zebrafish. *Dev. Cell* **29**, 350–359 (2014).

63. A.-L. Duchemin, H. Vignes, J. Vermot, Mechanically activated piezo channels modulate outflow tract valve development through the Yap1 and Klf2-Notch signaling axis. *eLife* **8**, e44706 (2019).

64. J. J. Hsu, V. Vedula, K. I. Baek, C. Chen, J. Chen, M. I. Chou, J. Lam, S. Subhedar, J. Wang, Y. Ding, C.-C. Chang, J. Lee, L. L. Demer, Y. Tintut, A. L. Marsden, T. K. Hsiai, Contractile and hemodynamic forces coordinate Notch1b-mediated outflow tract valve formation. *JCI Insight* **4**, e124460 (2019).

65. E. Zuniga, F. Stellabotte, J. G. Crump, Jagged-Notch signaling ensures dorsal skeletal identity in the vertebrate face. *Dev. Camb. Engl.* **137**, 1843 (2010).

66. C. B. Kimmel, W. W. Ballard, S. R. Kimmel, B. Ullmann, T. F. Schilling, Stages of embryonic development of the zebrafish. *Dev. Dyn.* **203**, 253–310 (1995).

67. B. Wong, Points of view: Color blindness. *Nat. Methods* **8**, 441–441 (2011).

Acknowledgments:
The authors thank the ERC, the Academy of Finland, InFLAMES Research Flagship Center and Åbo Akademi University for their financial support; The Swedish Cultural Foundation in Finland and Instrumentarium Science Foundation for financially supporting the work of FSR; J. G. Crump (University of Southern California, Keck School of Medicine) for generously providing us with Jagged1b (b1105) zebrafish embryos; N. Ninov (Center for Regenerative Therapies Dresden (CRTD) at TUD Dresden University of Technology) for kindly providing us with TP1:H2B-mCherry zebrafish embryos; Cell Imaging and Cytometry Core (Turku Bioscience Centre and Biocenter Finland) for providing training and imaging facilities. I. Patero and the Zebrafish Core (Turku Bioscience Centre) for providing training and the facilities for the in vivo experiments on zebrafish; E. Långbacka, J. Chenglim Liu and A. Viitala (Åbo Akademi University) for their technical support. Figures were created with BioRender.com.

Funding:

This project has received funding from the following sources:

European Research Council (ERC) and the European Union's Horizon 2020 research and innovation program grant agreement No 771168 (ForceMorph)

Research Council of Finland, decision number #316882 (SPACE)

Research Council of Finland, decision number #330411 (SignalSheets)

Research Council of Finland, decision number #336355 (Solutions for Health at Åbo Akademi University)

Research Council of Finland, decision number #337531 and #357911 (InFLAMES Flagship Program)

Åbo Akademi University Foundation's Centers of Excellence in Cellular Mechanostasis (CellMech) and Bioelectronic Activation of Cell Functions (BACE)

The work performed by FSR has been partially funded by personal grants from The Swedish Cultural Foundation in Finland and Instrumentarium Science Foundation

Author contributions:
Conceptualization: FSR and CMS

Methodology: RCHD, FZ and OMJAS

Investigation: FSR, NV, EK, RCHD, FZ and OMJAS

Formal analysis: FSR, NV, EK, RCHD, FZ, OMJAS and CMS

Resources: CVCB and CMS

Data curation: OMJAS and FSR

Writing – original draft: FSR and CMS

Writing – review & editing: FSR, NV, EK, RCHD, FZ, CVCB, OMJAS and CMS

Visualization: FSR

Supervision: CVCB, OMJAS and CMS

Project administration: FSR and CMS

Funding acquisition: CVCB and CMS

Competing interests:

Authors declare that they have no competing interests.

Data and materials availability:

All data, code, and materials used in the analysis will be available in an open repository once the final form of the manuscript is approved for publication. All other data are available in the main text or the supplementary materials.

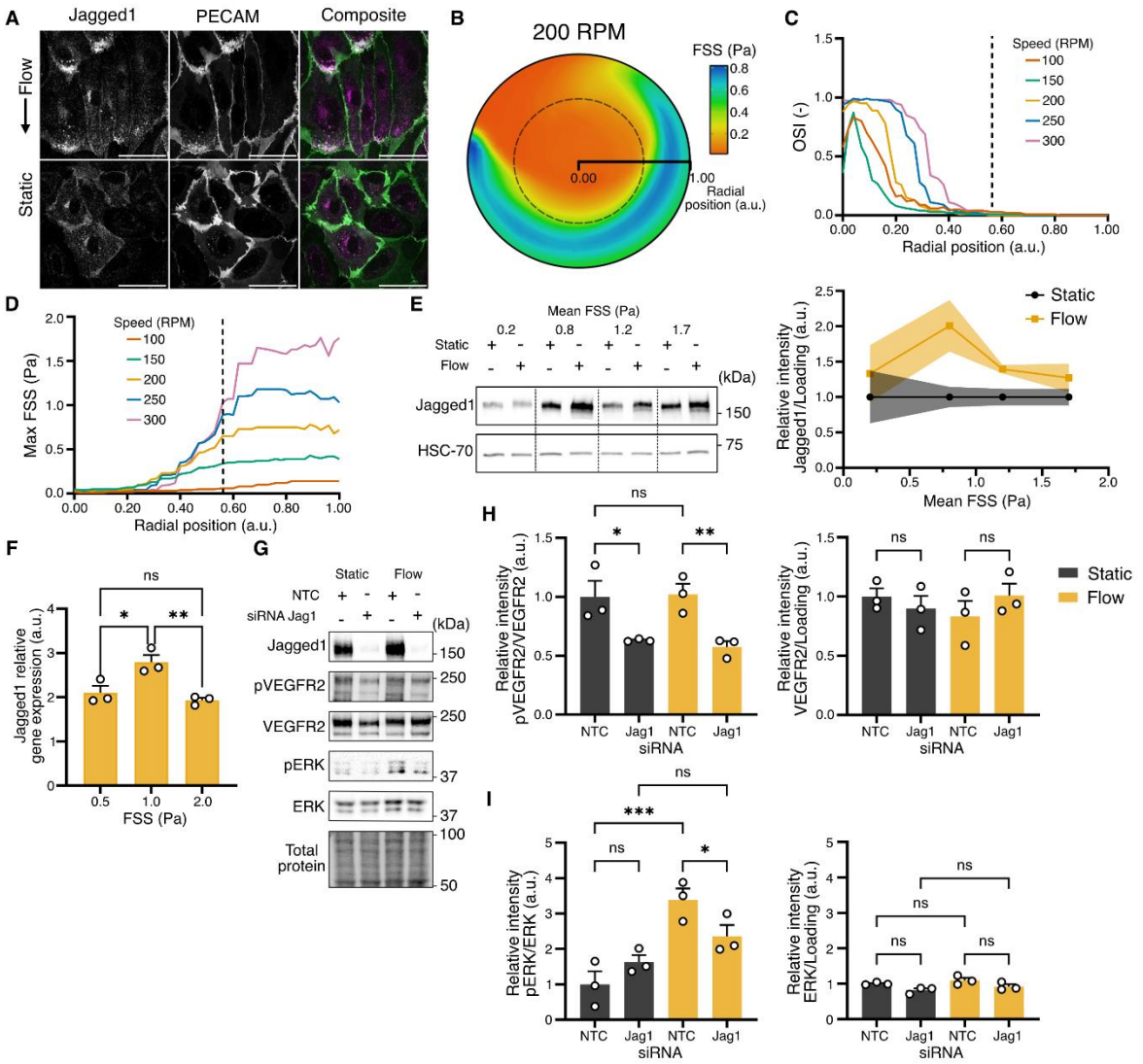

Fig. 1. Shear stress induces polarization and magnitude-dependent changes in Jag1 expression and Jag1 silencing alters shear stress signaling. (**A**) Confocal microscopy images of HAoECs exposed to 1.4 Pa laminar and continuous FSS for 24 hours in Ibidi microfluidic chips. Jag1 (magenta) demonstrated polarized localization in the direction of flow. PECAM/CD31 (green) was used to denote cell junctions. (**B**) Computational fluid dynamic analysis of the FSS pattern in an orbital shaker system using 6-well plates. The radial position indicates the radial coordinates of the well, with 0.00 indicating the center of the well and 1.00 the wall of the well. The dotted line separates the wells' outer area with high magnitude laminar flow from the inner area with highly oscillatory flow. Cells were collected from the outer area of the well, from radial position 0.56 to 1.00. (**C**) Oscillatory shear index (OSI) was calculated from the simulation and used to determine the zones with the lowest oscillatory flow. (**D**) Maximum FSS levels were used to determine the magnitude of FSS at each speed (RPM). (**E**) WB analysis of Jag1 protein levels in HUVECs exposed to different magnitudes of FSS using our orbital shaker system. The values are presented relative to the corresponding static control. (**F**) Q-PCR analysis of Jag1 gene expression levels in HUVECs exposed to laminar and continuous FSS of different magnitudes for 24 hours in Ibidi microfluidic chips. (**G**) WB of the phosphorylation and protein expression levels of VEGFR2 and ERK in HUVECs exposed to 0.8 Pa of FSS in the orbital shaker. Cells were silenced for 48 hours with siRNA non-targeting control (NTC) or siRNA Jag1 before exposure to FSS for 24 hours. Quantification of these experiments is found in (**H**) for VEGFR2 and (**I**) for ERK. All experiments were performed three times, for D this included three technical replicates within each experiment. The levels are presented as the mean of each replicate relative to their corresponding control + standard error of the mean (SEM). For WBs HSC-70 or total protein stainings were used as a loading control. P-values were obtained with GraphPad Prism as described in the methodology. Significance is indicated as: ns $p > 0.05$, * $p < 0.05$, ** $p < 0.01$, *** $p < 0.001$. Arbitrary units are indicated as (a.u.).

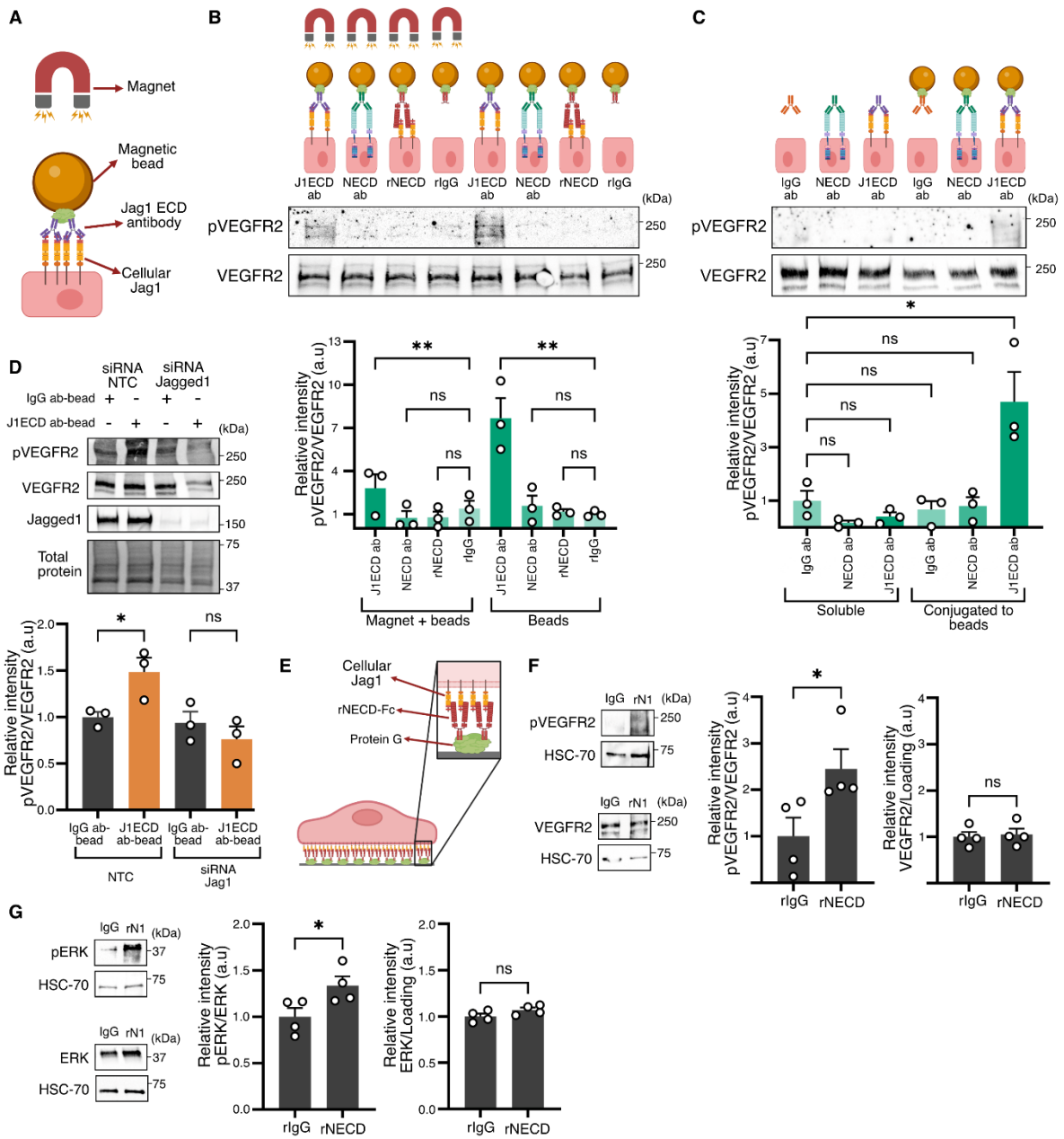

Fig. 2. Mechanical stimulation of Jag1 activates shear stress signaling. (**A**) Schematic illustration (not to scale) of the magnetic bead experiment: HUVECs were incubated with protein A/G magnetic beads coated with Jag1 extracellular domain (ECD) antibodies, (J1ECD ab), Notch ECD antibodies (NECD ab), recombinant Notch ECD (rNECD), or recombinant IgG (rIgG) for 15 minutes and then exposed to a magnet or incubated with the cells for a total of 30 minutes. (**B**) Western blot analysis of VEGFR2 and phosphorylated VEGFR2 in HUVECs treated with magnetic beads coated with J1ECD ab, NECD ab, rNECD, or rIgG. VEGFR2 phosphorylation was induced only in cells incubated with magnetic beads coated with the Jag1ECD antibody. (**C**) WB analysis of VEGFR2 and phosphorylated VEGFR2 in HUVECs treated with soluble J1ECD ab, NECD ab, or IgG ab or conjugated to magnetic beads. J1ECD ab-coated beads but not soluble Jag1 antibodies induced VEGFR2 phosphorylation. (**D**) WB analysis of VEGFR2 and phosphorylated VEGFR2 in control and Jag1-silenced HUVECs stimulated by J1ECD ab- or IgG ab-coated beads. siRNA-mediated silencing of Jag1 inhibited phosphorylation of VEGFR2 induced by the J1ECD ab-coated beads. (**E**) Schematic illustration of the experimental setup: HUVECs were cultured for six hours on top of rIgG or rNECD immobilized to protein G-coated culture dishes. (**F**) WB analysis of phosphorylated and total VEGFR2 and (**G**) ERK levels in HUVECs cultured on rIgG or rNECD. The levels are presented as the mean of each replicate relative to their corresponding control+ SEM. HSC-70 and whole cell lysates were used as a loading control. P-values were obtained with GraphPad Prism as described in the methodology. Significance is indicated as: ns $p > 0.05$, * $p < 0.05$, ** $p < 0.01$, *** $p < 0.001$. Arbitrary units are indicated as (a.u.).

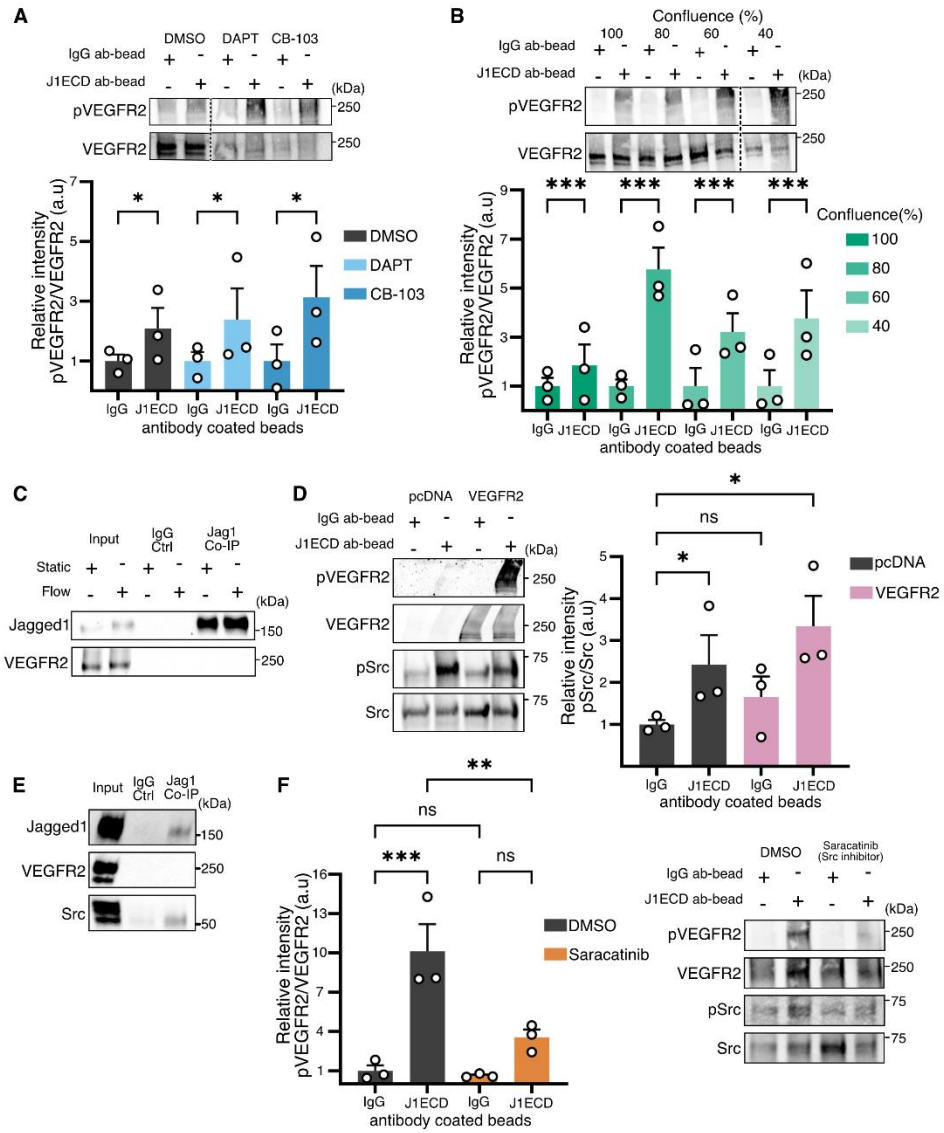

Fig. 3. Jag1-mediated VEGFR2 activation requires Src but is independent of Notch and the junctional mechanosensory complex. (**A**) WB analysis of phosphorylated and total VEGFR2 in HUVECs treated with J1ECD ab- or IgG ab-beads in the absence and presence of Notch pathway inhibitors. Pretreatment with Notch inhibitors DAPT and CB-103 did not reduce the Jag1-mediated VEGFR2 response. Values were normalized to the IgG ab-bead control. (**B**) WB analysis of phosphorylated and total VEGFR2 in HUVECs of different confluences treated with J1ECD ab- or IgG ab-coated beads. J1ECD ab-coated beads induced VEGFR2 activation did not decline with decreasing confluence in HUVECs. The values were normalized to the IgG ab-coated bead control for each confluence. (**C**) Jag1 Co-Immunoprecipitation (Co-IP) analysis by WB, of VEGFR2 in HUVECs cultured in static conditions or exposed to flow (0.8 Pa FSS) using the orbital shaker system. No VEGFR2 was detected in Jag1 Co-IP samples. (**D**) WB analysis of total and phosphorylated VEGFR2 and Src in Cos-7 stimulated with J1ECD ab- or IgG ab-coated beads after being transfected with plasmid control (pcDNA) or VEGFR2 expression plasmid. Stimulation of Cos-7 cells with J1ECD ab-coated beads induced Src and VEGFR2 activation. Src was activated in the absence of VEGFR2. The values were normalized to the IgG ab-bead control. (**E**) Jag1 Co-IP analysis by WB of VEGFR2 and Src in HUVECs cultured in static conditions. Src but not VEGFR2 are detected in Jag1 Co-IP samples. (**F**) WB analysis of phosphorylated and total VEGFR2 and Src in HUVECs stimulated with J1ECD ab- or IgG ab-coated beads in the presence and absence of the Src inhibitor Saracatinib. The values were normalized to the IgG bead control. The levels are presented as the mean of each replicate relative to their corresponding control + SEM. P-values were obtained with GraphPad Prism as described in the methodology. Significance is indicated as: ns $p > 0.05$, * $p < 0.05$, ** $p < 0.01$, *** $p < 0.001$. Arbitrary units are indicated as (a.u.).

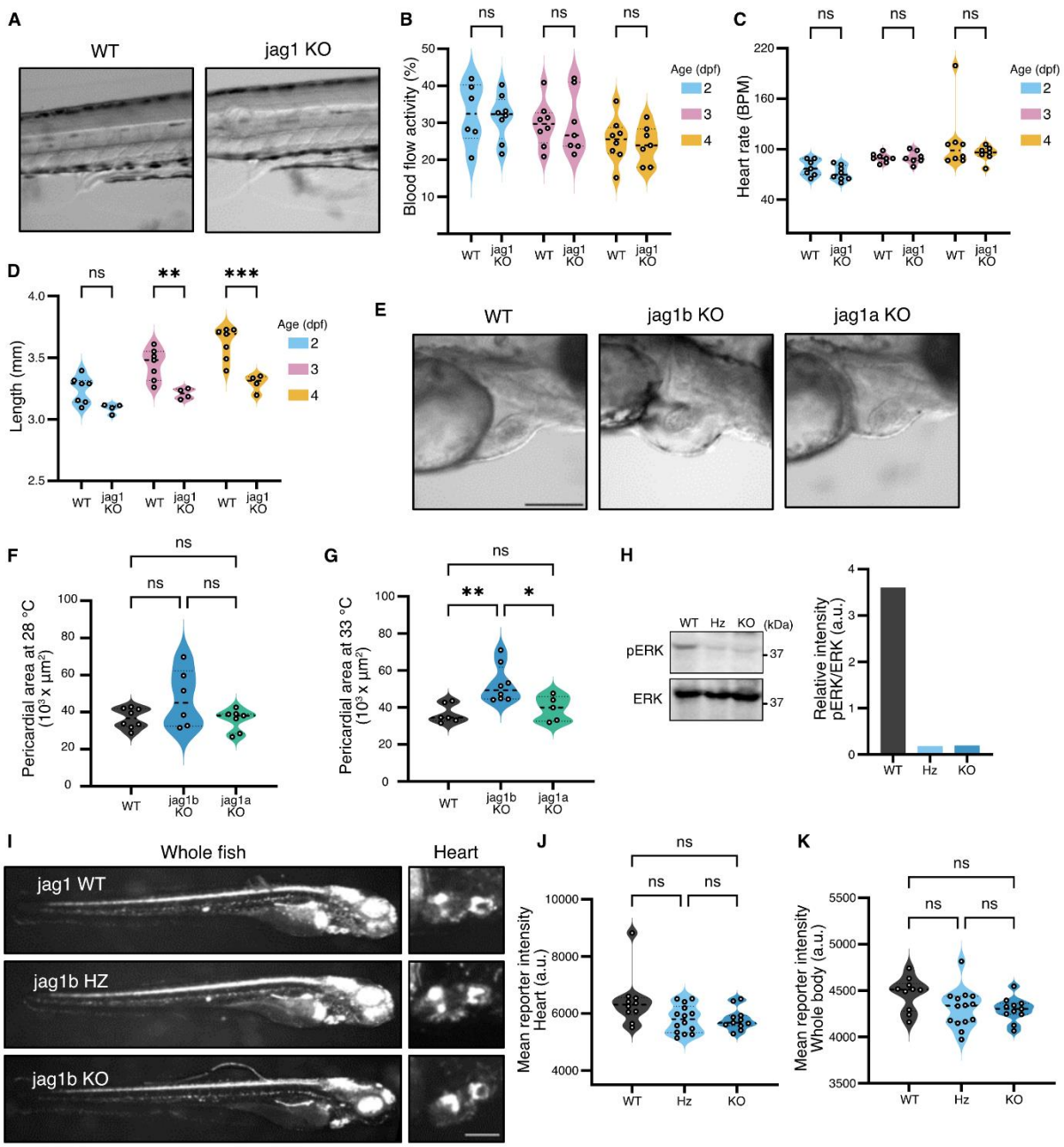

Fig. 4. **Deletion of jag1b in zebrafish leads to decreased ERK activity and pericardial edema**. (**A**) Representative light microscopy image of the notochord of Jag1 wildtype (WT) and jag1a/1b KO (jag1KO) zebrafish at 4 days post fertilization (dpf). (**B**) Blood flow activity in Jag1WT and KO zebrafish at 2, 3 and 4 dpf. (**C**) Heart rate in Jag1 WT and KO zebrafish at 2, 3 and 4 dpf. (**D**) Axial length of Jag1WT and KO zebrafish embryos at 2, 3 and 4 dpf. (**E**) Representative microscopy images of the developing heart in WT, Jag1a and Jag1b KO zebrafish at 4 dpf. jag1bKO zebrafish show signs of Pericardial edema. Scale bar: 200 µm. (**F**) Quantification of the pericardial area in Jag1WT, jag1bKO and jag1aKO zebrafish at 4dpf at 28°C and (**G**) 33°C. (**H**) ERK activity was measured in protein lysates of 10 WT, heterozygous (Hz) and homozygous Jag1KO (KO) embryos by Western Blotting. (**I**) Fluorescence images of Notch activity (TP1:H2B-mCherry) in TP1:H2B-mCherry (Jag1 WT); TP1:H2B-mCherry/jag1bHz and TP1:H2B-mCherry/jag1bKO zebrafish at 4 dpf. Scale bar: 200 µm for the heart. Quantification of Notch activity in the heart (**J**) and) the whole fish (**K)** was performed by measuring fluorescent intensity. P-values were obtained with GraphPad Prism as described in the methodology. Significance is indicated as: ns $p > 0.05$, * $p < 0.05$, ** $p < 0.01$, *** $p < 0.001$. Arbitrary units are indicated as (a.u.).